Is Wave Function Collapse Necessary? Explaining Quantum Nondemolition Measurement of a Spin Qubit within Linear Evolution

Harry E. Dyte,[1] George Gillard,[1] Santanu Manna,[2] Saimon F. Covre da Silva,[2] Armando Rastelli,[2] and Evgeny A. Chekhovich[1,3,*]

[1]*Department of Physics and Astronomy, University of Sheffield, Sheffield S3 7RH, United Kingdom*
[2]*Institute of Semiconductor and Solid State Physics, Johannes Kepler University Linz, Altenberger Strasse 69, 4040 Linz, Austria*
[3]*Department of Physics and Astronomy, University of Sussex, Brighton BN1 9QH, United Kingdom*

(Received 4 July 2023; revised 28 January 2024; accepted 14 March 2024; published 19 April 2024)

The measurement problem dates back to the dawn of quantum mechanics. Here, we measure a quantum dot electron spin qubit through off-resonant coupling with a highly redundant ancilla, consisting of thousands of nuclear spins. Large redundancy allows for single-shot measurement with high fidelity $\approx 99.85\%$. Repeated measurements enable heralded initialization of the qubit and backaction-free detection of electron spin quantum jumps, attributed to burstlike fluctuations in a thermally populated phonon bath. Based on these results we argue that the measurement, linking quantum states to classical observables, can be made without any "wave function collapse" in agreement with the Quantum Darwinism concept.

DOI: 10.1103/PhysRevLett.132.160804

High fidelity qubit readout is essential in quantum information processing. Usually, such readout starts with conversion of a fragile quantum state into a more robust form, detectable by a classical apparatus. Some readout techniques rely on high-energy excitations, making this conversion dissipative (irreversible). Examples include spin-to-charge conversion [1–4], single photon detection [5], optical readout of spin in defects [6–11], and quantum dots (QDs) [12–14]. An alternative is unitary (reversible) conversion. One example is the off-resonant (Ising) coupling between the main and ancilla electron spin qubits, which enables quantum nondemolition (QND) measurement [15]. Other QND demonstrations include superconducting qubits under off-resonant (dispersive-regime) coupling [16] and mechanical resonators [17].

Here, we implement unitary conversion of a QD electron spin, but the off-resonant ancilla consists of $\approx 10^4$–10^5 low-energy nuclear spin qubits. The large redundancy of the ancilla results in a very high measurement fidelity. Moreover, the method is particularly robust and simple to implement, since the nuclei are essentially the same in all QDs, eliminating the need for QD-specific calibrations. Addressing the controversial measurement problem, we argue that high fidelity is what an observer perceives as a deterministic classical outcome of a measurement. Crucially, in our system, the transition from the microscopic quantum-mechanical evolution to this perceived determinism is achieved without requiring any nonunitary wave function reduction ("collapse").

We study epitaxial GaAs/AlGaAs QDs [18–22] in a p-i-n diode structure, where bias tuning can inject individual electrons from the n-type Fermi reservoir [Fig. 1(b)]. A static magnetic field B_z is applied along the growth axis z. A typical QD consists of $N \approx 10^5$ atoms, whose nuclei are spin-3/2 particles. The sample is subject to uniaxial stress, which induces nuclear quadrupolar shifts [23]. This isolates the two-level subspace with spin projections $I_z = -3/2, -1/2$, allowing the nuclei to be treated as effective spin-1/2 particles. Individual QDs are addressed optically using focused laser excitation and photoluminescence (PL) spectroscopy. A copper coil is used to generate a radiofrequency (rf) magnetic field orthogonal to B_z. (See further details in Supplemental Material, Secs. 1 and 3 [24].)

The quantum system of a QD charged with a single electron ($1e$) is described with reference to the level diagram in Fig. 1(a). The hyperfine interaction Hamiltonian is $\mathcal{H}_{\rm hf} = \Sigma_k a_k \hat{\mathbf{s}} \cdot \hat{\mathbf{I}}_k$, where a_k describes the coupling between the spin vector $\mathbf{s}$ of the resident electron and the kth nuclear spin vector $\mathbf{I}_k$. This interaction has a twofold effect. First, in addition to the bare Larmor frequency $\nu_{\rm N}$, each nucleus acquires a Knight [53] frequency shift $s_z a_k/(2h)$. Second, the electron states with $s_z = \pm 1/2$ acquire the (Overhauser) hyperfine shifts $\pm E_{\rm hf}/2$, arising from the net polarization of the nuclear spin ensemble [Fig. 1(d)]. The average hyperfine shift is defined as $E_{\rm hf} = \Sigma_k a_k \langle \hat{I}_{z,k} \rangle$, where $\langle \ldots \rangle$ is the expectation

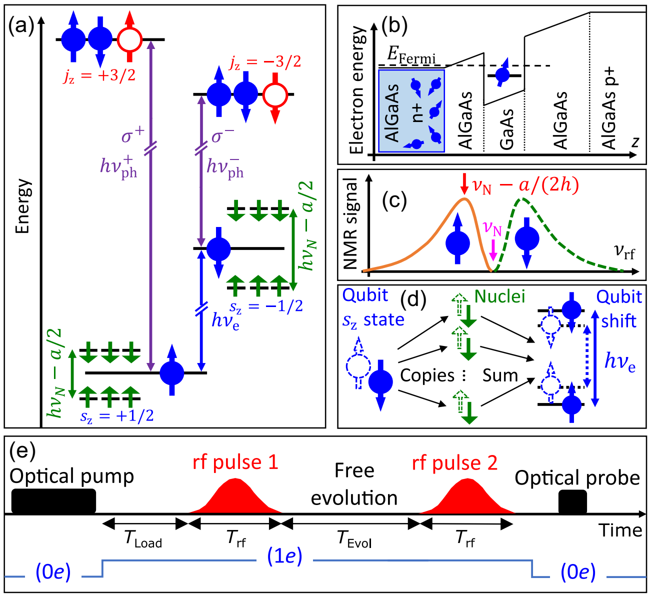

FIG. 1. (a) Energy level diagram of the nuclear spins (short green arrows), the electron (solid blue circle and arrow), and the optically excited trion, containing one hole (open red circle and arrow) and two electrons. (b) Conduction band energy diagram of the semiconductor structure, showing the GaAs quantum dot, AlGaAs barriers, and the doped AlGaAs layers. (c) The solid (dashed) curve shows schematically the nuclear magnetic resonance spectrum in the presence of a spin-up (spin-down) electron. Vertical arrows show the bare nuclear frequency ν_N and the frequency $\nu_N - a/(2h)$ of the detuned radiofrequency (rf) pulse. (d) The electron spin qubit projection is first copied into multiple nuclear spin ancillae by the rf pulse. The total nuclear polarization is then measured from the hyperfine shifts $E_{\rm hf}$ in the time-averaged PL spectra. (e) Timing diagram showing optical pump and probe, rf pulses, and the switching of the QD between the neutral $(0e)$ and electron-charged $(1e)$ states.

value. The electron spin energy splitting $h\nu_e$, is the sum of $E_{\rm hf}$ and the bare Zeeman splitting $h\nu_{e,0} = \mu_B g_e B_z$, where $g_e \approx -0.1$ is the electron g-factor and μ_B is the Bohr magneton. The optically excited trion contains a spin-singlet pair of electrons and an unpaired valence band hole with momentum projection $j_z = \pm 3/2$. Because of the selection rules, there are two dipole-allowed circularly polarized $(\sigma^\pm)$ optical transitions with photon energies $h\nu_{\rm ph}^\pm$. The optically detected spectral splitting $\Delta E_{\rm PL} = h(\nu_{\rm ph}^+ - \nu_{\rm ph}^-)$ yields $E_{\rm hf}$ [54].

Traditional readout uses resonant driving of a cyclic optical transition [e.g., σ^+ in Fig. 1(a)] to convert the electron spin state into the presence or absence of scattered photons [12–14]. However, there is a finite probability for the measurement process to destroy the spin qubit if the recombination goes via one of the "forbidden" channels [e.g., from $j_z = +3/2$ to $s_z = -1/2$ in Fig. 1(a)]. Here, we take a different approach, using the long coherence of the nuclear spins [55] and the large energy detunings $\nu_{\rm ph}^\pm \gg \nu_e \gg \nu_N$ to turn the nuclei into a QND measurement apparatus.

Figure 1(e) shows the timing diagram of the measurement cycle. It starts with a long (few seconds) circularly polarized optical pumping of an empty $(0e)$ QD, which polarizes the nuclear spins up to $\approx 80\%$ [56,57]. Next, an electron is loaded from the Fermi reservoir $(1e)$ and is allowed to equilibrate for a time $T_{\rm Load}$. Nuclear magnetic resonance (NMR) is performed by applying a rf pulse with a total duration $T_{\rm rf}$, calibrated to induce a π rotation of the nuclear spins. In some experiments, a second rf pulse is applied, following a free evolution time $T_{\rm Evol}$. The final step is the illumination of the QD with a short (tens of milliseconds) continuous wave optical probe in order to collect the PL spectrum and derive $E_{\rm hf}$. Importantly, all measurements are done in one cycle, i.e., for the electron spin projection s_z the measurement is single-shot.

The readout of the electron spin qubit is explained in Fig. 1(c). An electron in state $s_z = +1/2$ $(-1/2)$ Knight-shifts the QD NMR spectrum to the lower (higher) frequency side of ν_N. A single rf pulse is applied at a radiofrequency $\nu_N - a/(2h)$, where a is a weighted average of a_k in a QD. For the electron in the $s_z = +1/2$ $(-1/2)$ state, the rf pulse is in (out of) resonance, so the QD nuclei are flipped (remain in the initial state) [6]. Statistics of the measured single-cycle PL probe spectra [Fig. 2(a)] show a clear bimodality in the spectral splitting (red and black traces), arising from the bimodal distribution of the rf-induced variation of the hyperfine shift $\Delta E_{\rm hf}$. A systematic dependence of $\Delta E_{\rm hf}$ on the rf detuning from ν_N is shown in Fig. 2(b), where the two branches corresponding to $s_z = +1/2$ and $-1/2$ are traced by the solid and dashed

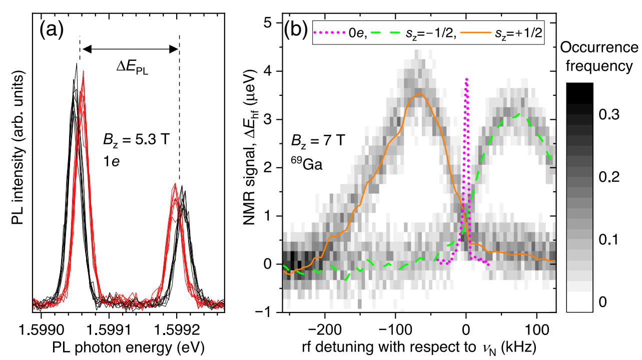

FIG. 2. (a) A random set of 16 probe PL spectra following the detuned rf π pulse applied to a charged $(1e)$ QD. The changes in the doublet splitting $\Delta E_{\rm PL}$ are due to the changes $\Delta E_{\rm hf}$ in the hyperfine shift $E_{\rm hf}$. The bimodality in $\Delta E_{\rm PL}$ (and $\Delta E_{\rm hf}$) corresponds to the two s_z states of the electron. (b) Histogram of the single-cycle NMR signals $\Delta E_{\rm hf}$ measured at variable detunings from the ^{69}Ga bare NMR frequency ν_N ($\nu_N \approx 72.15$ MHz at $B_z \approx 7$ T). The solid (dashed) line traces the branch of the NMR resonance corresponding to the $s_z = +1/2$ $(-1/2)$ electron spin state. The dotted line shows the same single-QD resonance but measured in a neutral charge state $(0e)$ via "inverse" NMR [58].

lines, respectively. The broadening of these traces arises from the inhomogeneous distribution of a_k, while in an empty QD ($0e$, dotted line) the broadening of the NMR spectrum is due to the much smaller quadrupolar inhomogeneity. The optimal resolution of the two electron spin states (the maximum difference in ΔE_{hf}) is observed when the rf detuning matches the typical Knight shift $a/(2h) \approx 70$ kHz.

Using the optimal detuning, we collect detailed statistics of the single-cycle NMR signals ΔE_{hf}. In an empty QD [$0e$, Fig. 3(a)] the distribution of ΔE_{hf} is a single mode, broadened by the noise in probe PL spectra. The mode is centered at a small $\Delta E_{\mathrm{hf}} \approx 1.7$ μeV, indicating partial rotation of the nuclei by the detuned rf pulse. The same measurement in a charged QD [$1e$, Fig. 3(b)] shows a bimodal distribution around two discrete values of ΔE_{hf}.

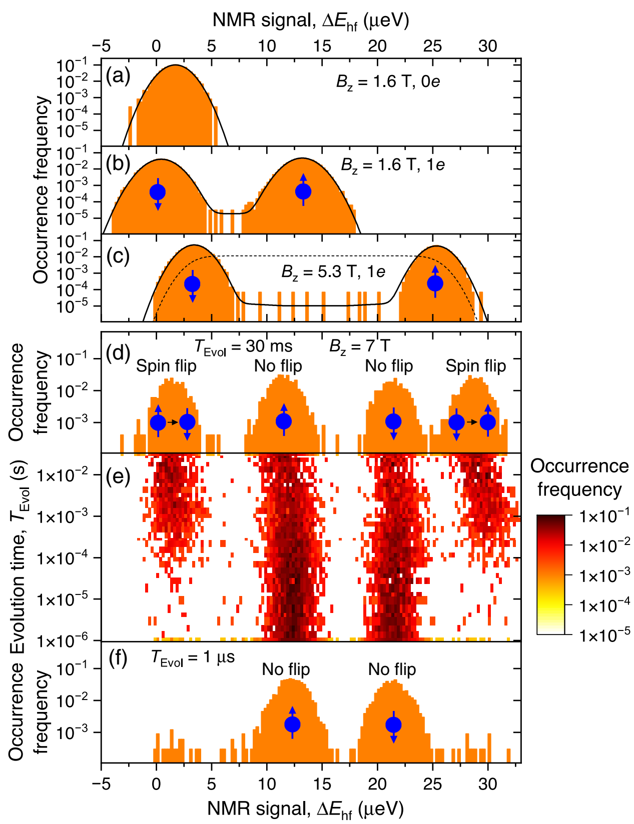

FIG. 3. (a),(b) Histograms of the single-cycle NMR signals ΔE_{hf} measured at $B_z = 1.6$ T on the same individual QD in a neutral charge state ($0e$, a), and in a single-electron charged state ($1e$, b). The NMR signals are produced by a single detuned rf π pulse. Solid lines show the best model fitting. (c) Same as (b) but on a different QD and at $B_z = 5.3$ T, where more efficient nuclear spin polarization results in a larger separation of the histogram modes. The dashed line shows a model distribution for a randomly oriented electron spin. (d),(e) Histograms of the single-cycle NMR signals ΔE_{hf} measured at $B_z = 7$ T with two rf π pulses applied to ^{75}As and ^{69}Ga and delayed by T_{Evol}. A full 2D histogram at variable T_{Evol} is shown in (e), while (d) and (f) show the cross sections at long and short T_{Evol}, respectively.

The mode centered at $\Delta E_{\mathrm{hf}} \approx 0.4$ μeV (≈13.2 μeV) corresponds to the $s_z = -1/2$ $(+1/2)$ state, where the electron Knight-shifts the nuclei out of (into) resonance with the rf pulse. Thus, the electron's quantum variable $\hat{s}_z$ is measured via single-shot optically detected NMR.

We note a small number of events where the NMR signal deviates from either of the modes [8 μeV $\lesssim \Delta E_{\mathrm{hf}} \lesssim$ 21 μeV in Fig. 3(c)]. We ascribe such intermediate readouts to electron spin flips during the rf pulse, resulting in partial rotation of the nuclear spins. We model this process by assuming a probability p_{Flip} for the electron spin to flip during T_{rf}. The optical readout noise is also included in the model (see Supplemental Material, Sec. 4 [24]). The best-fit results are shown by the solid lines in Figs. 3(b) and 3(c). Using the fitted mode positions $\Delta E_{\mathrm{hf}}^{-}$ and $\Delta E_{\mathrm{hf}}^{+}$, we set the threshold at $(\Delta E_{\mathrm{hf}}^{-} + \Delta E_{\mathrm{hf}}^{+})/2$ and calculate the probability that the detected ΔE_{hf} is below (above) the threshold when the electron state is $s_z = -1/2$ $(+1/2)$. This probability is the qubit readout fidelity, found to be $F \approx 0.9985$, matching or exceeding the state of the art in a range of qubit systems [2,8,10,11,59]. Since the two histogram modes are well resolved, the loss of fidelity is dominated by the random electron spin flips, leading to $F \approx 1 - p_{\mathrm{Flip}}/2 \approx 1 - T_{\mathrm{rf}}/(4T_{1,\mathrm{e}})$, where $T_{1,\mathrm{e}}$ is the electron spin lifetime. Nuclear spin relaxation ($T_{1,\mathrm{N}} \approx 1$–10 s [21]) and decoherence ($T_{2,\mathrm{N}} \approx 1$ ms [55]) are slow, and therefore do not limit the choice of T_{rf}. The lower limit $T_{\mathrm{rf}} \gtrsim h/a$ comes from the need to resolve the $s_z = \pm 1/2$ Knight-shifted NMR spectra with a short (spectrally broad) rf pulse. Our experiments with $T_{\mathrm{rf}} \approx 10$–20 μs are already close to this limit, constrained by the QD size through $a \propto N^{-1}$. The other limitation comes from $T_{1,\mathrm{e}}$, which ranges from milliseconds to tens of milliseconds for temperature $T \approx 4.2$ K and our typical electron spin splitting $h\nu_{\mathrm{e}} \approx 50$ μeV. Further increase in $T_{1,\mathrm{e}}$ (and hence increase in F) can be achieved by lowering the temperature toward $k_{\mathrm{B}}T \approx h\nu_{\mathrm{e}}$, and by lowering $h\nu_{\mathrm{e}}$ through reduced magnetic field and nuclear spin polarization.

Immediate repeatability is a key requirement for any measurement [60,61], which we verify in an experiment with two rf pulses [Fig. 1(e)]. The first pulse applied to ^{75}As nuclei records the initial state, while the second pulse on ^{69}Ga stores the s_z state after the interpulse delay T_{Evol}. The optically measured ΔE_{hf} is the total NMR signal produced by the two pulses. Figure 3(e) shows a two-dimensional histogram of ΔE_{hf} measured at different T_{Evol}. A cross section at short $T_{\mathrm{Evol}} \approx 1$ μs [Fig. 3(f)] reveals the same bimodal distribution as in Figs. 3(b) and 3(c), with only two "no-flip" modes corresponding to $s_z = \pm 1/2$. This shows that the measured observable $\hat{s}_z$ is not altered by the rf pulses, confirming the QND character of the measurement [60]. The two additional "spin-flip" modes, corresponding to s_z inversion during T_{Evol}, emerge only at long T_{Evol} [≈30 ms in Fig. 3(d)]. Analysis of the entire T_{Evol} dependence reveals the spin lifetime $T_{1,\mathrm{e}} \approx 0.58$ ms at

$B_z = 7$ T, measured in equilibrium without any active initialization of the electron spin. Instead, a heralded initialization is performed by the first rf pulse, which stores the initial s_z in the ^{75}As polarization, to be retrieved by the optical probe afterward.

The readout time $T_{\mathrm{rf}} = 20$ μs is short enough to follow the electron spin evolution on the timescale of $T_{1,\mathrm{e}}$. However, Fig. 3(e) shows that the electron spin is nearly always detected in either of the eigenstates $s_z = \pm 1/2$, with very rare intermediate NMR readouts ΔE_{hf}. This suggests a random telegraph process, where the electron is in one of the eigenstates $s_z = \pm 1/2$ most of the time, occasionally experiencing quantum jumps that are much faster than T_{rf}.

We gain further insight with the aid of the first-principle numerical modeling, where the Schrödinger equation is propagated from the initial wave function state ψ_{Init} into the final state ψ_{Fin} (see details in Supplemental Material, Sec. 6 [24]). Initially the nuclei are in a polarized state and the electron spin is in a general superposition $\psi_{\mathrm{Init}} = \alpha|+1/2\rangle + \beta|-1/2\rangle$ with the z-projection expectation value $s_{\mathrm{z,Init}} = (|\alpha|^2 - |\beta|^2)/2$. Following the detuned rf pulse, we find that (i) the final polarization of each nucleus equals the initial electron polarization $I_{\mathrm{z},k,\mathrm{Fin}} \approx s_{\mathrm{z,Init}}$ and (ii) the electron polarization is nearly unchanged $s_{\mathrm{z,Fin}} \approx s_{\mathrm{z,Init}}$. Such nondemolition copying of the quantum variable $\hat{s}_z$ comes at the expense of completely erasing the conjugate variable [60], which manifests in $s_{\mathrm{x,Fin}} \approx s_{\mathrm{y,Fin}} \approx 0$ regardless of the initial electron state. This is in agreement with the no-cloning theorem, since only s_z is copied, but not the entire spin state of the electron. These results can be understood qualitatively through the large detuning $\nu_{\mathrm{N}} \ll \nu_{\mathrm{e}}$, meaning that the nuclei sense only the slowly varying average electron polarization s_z. Conversely, since $\nu_{\mathrm{e}} > N\nu_{\mathrm{N}}$ the nuclei do not have enough energy to flip the electron spin, which therefore follows adiabatically any rf-induced evolution of the nuclear spin polarization [62].

If all electron spin superpositions had equal probabilities, the linear response of the measurement apparatus $I_{\mathrm{z},k,\mathrm{Fin}} \approx s_{\mathrm{z,Init}}$ would have resulted in a nearly uniform distribution of the single-shot NMR signals, calculated and shown by the dashed line in Fig. 3(c). And yet the measurements yield a sharp bimodal distribution, revealing the energy eigenstates $s_z = \pm 1/2$ as a preferential basis. Quantum mechanics does not prescribe any preferential eigenbasis toward which the superpositions should decohere. Such a preferential basis can arise from the interaction of the qubit with the environment, known as einselection [61,63]. The nuclear spin environment has been ruled out above—its energy is too small to "project" the high-energy electron spin qubit into the $s_z = \pm 1/2$ eigenstates. We also argue that "projection" of nuclear spin polarization itself, e.g., by the optical probe, is unlikely (Supplemental Material, Sec. 3C [24]). By contrast, the lattice vibrations (phonons) are known to be the high-energy environment that drives electron spin relaxation, enabled by spin-orbit mixing [64–70]. We therefore conjecture that the phonons are responsible for einselection and quantum jumps.

The inverse dependence of $T_{1,\mathrm{e}}$ on B_z (see Supplemental Material, Sec. 5 [24]) confirms the dominant role of the phonons [64–70]. The effective spin-phonon coupling is $\propto (\hat{s}_x \mathcal{E}_x - \hat{s}_y \mathcal{E}_y)$, where $\mathcal{E}_{x,y}$ are the Cartesian components of the phonon-induced piezo-strain electric field [64]. This form of interaction suggests that electron spin quantum jumps are driven by quasiresonant electric fields, occurring in the form of short ($\ll 10$ μs) random bursts, separated by long (milliseconds) random intervals. The QND nature of the measurement assures that the observed jumps are a spontaneous equilibrium process [71], as opposed to previous QD studies [8,13], where the observation process (continuous optical excitation) could itself induce the qubit jumps. Spontaneous collapses and burstlike revivals have been investigated in bosonic systems, such as photons [72] and phonons [73,74], and are typically associated with high mode population numbers $\bar{n} \gtrsim 100$. The appearance of spontaneous revivals at much lower average phonon numbers $\bar{n} \approx 6.8$ (for $T = 4.2$ K and $h\nu_{\mathrm{e}} \approx 50$ μeV used here) is somewhat unexpected, calling for further investigation.

The measurement time $T_{\mathrm{rf}} \approx 10$–$20$ μs is short compared both to $T_{1,\mathrm{e}}$ and the electron spin coherence time $T_{2,\mathrm{e}} \approx 100$ μs [22]. Thus, our QND readout method should allow for single-shot probing of the electron spin coherence without the burden of dynamical decoupling, required in time-averaged measurements. Conversely, a detuned rf pulse can be used to generate and study the Greenberger-Horne-Zeilinger (Schrödinger cat) nuclear states.

Finally, we discuss the broader implications of our experiments. The interpretation of quantum mechanics is a long-standing and controversial topic. The measurement problem is one of its manifestations, seeking to understand how linear quantum-mechanical evolution of the wave function turns into classical discrete measurement outcomes. Radically different hypotheses range from dynamical reduction models, which argue for nonlinear evolution and real wave function collapse, e.g., due to gravity [75], to models such as Quantum Darwinism [61,76], which seek an explanation within the standard linear evolution (see Supplemental Material, Sec. 7 [24]). At present, no experiment can resolve this dilemma. Hence, our analysis, presented below, should be treated as an open invitation for further academic debate. We argue that our results support the Quantum Darwinism perspective. While we cannot rule out wave function collapses, if only because we cannot verify effects such as gravity, we argue that such "collapses" are not necessary to describe our experiments. Our quantum system benefits from an accurate microscopic picture of the couplings between the electron, the nuclei, and the rf fields, as well as the excellent isolation of the nuclear spins from the solid state environments [21,55]. This permits a purely linear-evolution description of the first stage of the measurement, where the fast ($T_{\mathrm{rf}} < T_{2,\mathrm{e}}, T_{2,\mathrm{N}}, T_{1,\mathrm{e}}, T_{1,\mathrm{N}}$) coherent rf pulse copies the electron state s_z into nuclear states $I_{z,k}$ [see Fig. 1(d)]. Thanks to the large number $\approx 10^4$–10^5 of nuclear copies, their arithmetic sum (nuclear magnetization) is essentially a classical variable, in a sense that it is not "collapsed" by the subsequent (second stage) optical measurement. Indeed, illumination by the probe laser degrades the nuclear magnetization, but only gradually, and slowly enough to generate $\approx 10^8$ PL photons (Supplemental Material, Sec. 3C [24]), whose hyperfine spectral shifts $\pm E_{\mathrm{hf}}/2$ return the measurement outcome for the $\hat{s}_z$ quantum variable. Since a nonunitary "wave function collapse" is not needed to describe the measurement in our system, we argue that it may be a mere simplification in other settings too, invoked because the microscopic picture is missing, for example if the measurement involves coupling of the qubit to a high-energy apparatus, such as optical fields.

H. E. D. was supported by an EPSRC doctoral training grant. E. A. C. was supported by a University Research Fellowship from the Royal Society. G. G. and E. A. C. were supported by EPSRC Grant No. EP/V048333/1. A. R. acknowledges support of the Austrian Science Fund (FWF) via the Research Group FG5, I 4320, I 4380, I 3762, the Linz Institute of Technology (LIT), and the LIT Secure and Correct Systems Lab, supported by the State of Upper Austria, the European Union's Horizon 2020 research and innovation program under Grant Agreements No. 899814 (Qurope), No. 871130 (Ascent+), the QuantERA II project QD-E-QKD, and the FFG (Grant No. 891366).

S. M., S. F. C. S., and A. R. developed, grew, and processed the quantum dot samples. H. E. D. and G. G. conducted the experiments. H. E. D., G. G., and E. A. C. analyzed the data. H. E. D., E. A. C., and G. G. drafted the manuscript with input from all authors. H. E. D. and G. G. contributed equally to this letter. E. A. C. performed numerical modeling and coordinated the project.

*Corresponding author: e.chekhovich@sussex.ac.uk

[1] J. M. Elzerman, R. Hanson, L. H. Willems van Beveren, B. Witkamp, L. M. K. Vandersypen, and L. P. Kouwenhoven, Single-shot read-out of an individual electron spin in a quantum dot, Nature (London) **430**, 431 (2004).

[2] B. Hensen, W. Wei Huang, C.-H. Yang, K. Wai Chan, J. Yoneda, T. Tanttu, F. E. Hudson, A. Laucht, K. M. Itoh, T. D. Ladd, A. Morello, and A. S. Dzurak, A silicon quantum-dot-coupled nuclear spin qubit, Nat. Nanotechnol. **15**, 13 (2020).

[3] T. Meunier, I. T. Vink, L. H. Willems van Beveren, F. H. L. Koppens, H. P. Tranitz, W. Wegscheider, L. P. Kouwenhoven, and L. M. K. Vandersypen, Nondestructive measurement of electron spins in a quantum dot, Phys. Rev. B **74**, 195303 (2006).

[4] M. Veldhorst, J. C. C. Hwang, C. H. Yang, A. W. Leenstra, B. de Ronde, J. P. Dehollain, J. T. Muhonen, F. E. Hudson, K. M. Itoh, A. Morello, and A. S. Dzurak, An addressable quantum dot qubit with fault-tolerant control-fidelity, Nat. Nanotechnol. **9**, 981 (2014).

[5] R. H. Hadfield, Single-photon detectors for optical quantum information applications, Nat. Photonics **3**, 696 (2009).

[6] L. Jiang, J. S. Hodges, J. R. Maze, P. Maurer, J. M. Taylor, D. G. Cory, P. R. Hemmer, R. L. Walsworth, A. Yacoby, A. S. Zibrov, and M. D. Lukin, Repetitive readout of a single electronic spin via quantum logic with nuclear spin ancillae, Science **326**, 267 (2009).

[7] L. Robledo, H. Bernien, T. v. d. Sar, and R. Hanson, Spin dynamics in the optical cycle of single nitrogen-vacancy centres in diamond, New J. Phys. **13**, 025013 (2011).

[8] M. Raha, S. Chen, C. M. Phenicie, S. Ourari, A. M. Dibos, and J. D. Thompson, Optical quantum nondemolition measurement of a single rare earth ion qubit, Nat. Commun. **11**, 1605 (2020).

[9] J. M. Kindem, A. Ruskuc, J. G. Bartholomew, J. Rochman, Y. Q. Huan, and A. Faraon, Control and single-shot readout of an ion embedded in a nanophotonic cavity, Nature (London) **580**, 201 (2020).

[10] R. E. Evans, M. K. Bhaskar, D. D. Sukachev, C. T. Nguyen, A. Sipahigil, M. J. Burek, B. Machielse, G. H. Zhang, A. S. Zibrov, E. Bielejec, H. Park, M. Lončar, and M. D. Lukin, Photon-mediated interactions between quantum emitters in a diamond nanocavity, Science **362**, 662 (2018).

[11] M. K. Bhaskar, R. Riedinger, B. Machielse, D. S. Levonian, C. T. Nguyen, E. N. Knall, H. Park, D. Englund, M. Lončar, D. D. Sukachev, and M. D. Lukin, Experimental demonstration of memory-enhanced quantum communication, Nature (London) **580**, 60 (2020).

[12] A. N. Vamivakas, C. Y. Lu, C. Matthiesen, Y. Zhao, S. Fält, A. Badolato, and M. Atatüre, Observation of spin-dependent quantum jumps via quantum dot resonance fluorescence, Nature (London) **467**, 297 (2010).

[13] A. Delteil, Wei-bo Gao, P. Fallahi, J. Miguel-Sanchez, and A. Imamoğlu, Observation of quantum jumps of a single quantum dot spin using submicrosecond single-shot optical readout, Phys. Rev. Lett. **112**, 116802 (2014).

[14] N. O. Antoniadis, M. R. Hogg, W. F. Stehl, A. Javadi, N. Tomm, R. Schott, S. R. Valentin, A. D. Wieck, A. Ludwig, and R. J. Warburton, Cavity-enhanced single-shot readout of a quantum dot spin within 3 nanoseconds, Nat. Commun. **14**, 3977 (2023).

[15] J. Yoneda, K. Takeda, A. Noiri, T. Nakajima, S. Li, J. Kamioka, T. Kodera, and S. Tarucha, Quantum nondemolition readout of an electron spin in silicon, Nat. Commun. **11**, 1144 (2020).

[16] A. Blais, R.-S. Huang, A. Wallraff, S. M. Girvin, and R. J. Schoelkopf, Cavity quantum electrodynamics for superconducting electrical circuits: An architecture for quantum computation, Phys. Rev. A **69**, 062320 (2004).

[17] M. Rossi, D. Mason, J. Chen, Y. Tsaturyan, and A. Schliesser, Measurement-based quantum control of mechanical motion, Nature (London) **563**, 53 (2018).

[18] C. Heyn, A. Stemmann, T. Koppen, C. Strelow, T. Kipp, M. Grave, S. Mendach, and W. Hansen, Highly uniform and strain-free GaAs quantum dots fabricated by filling of self-assembled nanoholes, Appl. Phys. Lett. **94**, 183113 (2009).

[19] P. Atkinson, E. Zallo, and O. G. Schmidt, Independent wavelength and density control of uniform GaAs/AlGaAs quantum dots grown by infilling self-assembled nanoholes, J. Appl. Phys. **112**, 054303 (2012).

[20] M. Gurioli, Z. Wang, A. Rastelli, T. Kuroda, and S. Sanguinetti, Droplet epitaxy of semiconductor nanostructures for quantum photonic devices, Nat. Mater. **18**, 799 (2019).

[21] P. Millington-Hotze, S. Manna, S. F. Covre da Silva, A. Rastelli, and E. A. Chekhovich, Nuclear spin diffusion in the central spin system of a GaAs/AlGaAs quantum dot, Nat. Commun. **14**, 2677 (2023).

[22] L. Zaporski, N. Shofer, J. H. Bodey, S. Manna, G. Gillard, M. H. Appel, C. Schimpf, S. F. Covre da Silva, J. Jarman, G. Delamare, G. Park, U. Haeusler, E. A. Chekhovich, A. Rastelli, D. A. Gangloff, M. Atatüre, and C. Le Gall, Ideal refocusing of an optically active spin qubit under strong hyperfine interactions, Nat. Nanotechnol. **18**, 257 (2023).

[23] E. A. Chekhovich, I. M. Griffiths, M. S. Skolnick, H. Huang, S. F. Covre da Silva, X. Yuan, and A. Rastelli, Cross calibration of deformation potentials and gradient-elastic tensors of GaAs using photoluminescence and nuclear magnetic resonance spectroscopy in GaAs/AlGaAs quantum dot structures, Phys. Rev. B **97**, 235311 (2018).

[24] See Supplemental Material at http://link.aps.org/supplemental/10.1103/PhysRevLett.132.160804 for additional information and discussion, which includes Refs. [25–52].

[25] A. Oshiyama and S. Ohnishi, DX center: Crossover of deep and shallow states in Si-doped $Al_xGa_{1-x}As$, Phys. Rev. B **33**, 4320 (1986).

[26] P. M. Mooney, Deep donor levels (DX centers) in III-V semiconductors, J. Appl. Phys. **67**, R1 (1990).

[27] L. Zhai, M. C. Löbl, G. N. Nguyen, J. Ritzmann, A. Javadi, C. Spinnler, A. D. Wieck, A. Ludwig, and R. J. Warburton, Low-noise GaAs quantum dots for quantum photonics, Nat. Commun. **11**, 4745 (2020).

[28] G. L. Bir and G. E. Pikus, *Symmetry and Strain-induced Effects in Semiconductors* (Wiley, New York, 1974).

[29] W. A. Coish and J. Baugh, Nuclear spins in nanostructures, Phys. Status Solidi (b) **246**, 2203 (2009).

[30] E. A. Chekhovich, S. F. C. da Silva, and A. Rastelli, Nuclear spin quantum register in an optically active semiconductor quantum dot, Nat. Nanotechnol. **15**, 999 (2020).

[31] C. P. Slichter, *Principles of Magnetic Resonance* (Springer, New York, 1990).

[32] A. Ulhaq, Q. Duan, E. Zallo, F. Ding, O. G. Schmidt, A. I. Tartakovskii, M. S. Skolnick, and E. A. Chekhovich, Vanishing electron g factor and long-lived nuclear spin polarization in weakly strained nanohole-filled GaAs/AlGaAs quantum dots, Phys. Rev. B **93**, 165306 (2016).

[33] E. A. Chekhovich, M. M. Glazov, A. B. Krysa, M. Hopkinson, P. Senellart, A. Lemaître, M. S. Skolnick, and A. I. Tartakovskii, Element-sensitive measurement of the hole-nuclear spin interaction in quantum dots, Nat. Phys. **9**, 74 (2013).

[34] D. Gammon, A. L. Efros, T. A. Kennedy, M. Rosen, D. S. Katzer, D. Park, S. W. Brown, V. L. Korenev, and I. A. Merkulov, Electron and nuclear spin interactions in the optical spectra of single GaAs quantum dots, Phys. Rev. Lett. **86**, 5176 (2001).

[35] B. Eble, O. Krebs, A. Lemaître, K. Kowalik, A. Kudelski, P. Voisin, B. Urbaszek, X. Marie, and T. Amand, Dynamic nuclear polarization of a single charge-tunable InAs/GaAs quantum dot, Phys. Rev. B **74**, 081306(R) (2006).

[36] J. Skiba-Szymanska, E. A. Chekhovich, A. V. Nikolaenko, A. I. Tartakovskii, M. N. Makhonin, I. Drouzas, M. S. Skolnick, and A. B. Krysa, Overhauser effect in individual $InP/Ga_xIn_{1-x}P$ dots, Phys. Rev. B **77**, 165338 (2008).

[37] G. Ragunathan, J. Kobak, G. Gillard, W. Pacuski, K. Sobczak, J. Borysiuk, M. S. Skolnick, and E. A. Chekhovich, Direct measurement of hyperfine shifts and radio frequency manipulation of nuclear spins in individual CdTe/ZnTe quantum dots, Phys. Rev. Lett. **122**, 096801 (2019).

[38] E. A. Chekhovich, M. Hopkinson, M. S. Skolnick, and A. I. Tartakovskii, Suppression of nuclear spin bath fluctuations in self-assembled quantum dots induced by inhomogeneous strain, Nat. Commun. **6**, 6348 (2015).

[39] M. Atature, J. Dreiser, A. Badolato, A. Hogele, K. Karrai, and A. Imamoğlu, Quantum-dot spin-state preparation with near-unity fidelity, Science **312**, 551 (2006).

[40] W. T. Wenckebach, The solid effect, Appl. Magn. Reson. **34**, 227 (2008).

[41] E. A. Chekhovich, M. N. Makhonin, K. V. Kavokin, A. B. Krysa, M. S. Skolnick, and A. I. Tartakovskii, Pumping of nuclear spins by optical excitation of spin-forbidden transitions in a quantum dot, Phys. Rev. Lett. **104**, 066804 (2010).

[42] C. Schimpf, M. Reindl, P. Klenovský, T. Fromherz, S. F. Covre Da Silva, J. Hofer, C. Schneider, S. Höfling, R. Trotta, and A. Rastelli, Resolving the temporal evolution of line broadening in single quantum emitters, Opt. Express **27**, 35290 (2019).

[43] C.-P. Yang, Y.-x. Liu, and F. Nori, Phase gate of one qubit simultaneously controlling n qubits in a cavity, Phys. Rev. A **81**, 062323 (2010).

[44] K. A. Serrels, E. Ramsay, P. A. Dalgarno, B. Gerardot, J. A. O'Connor, R. H. Hadfield, R. J. Warburton, and D. T. Reid, Solid immersion lens applications for nanophotonic devices, J. Nanophoton. **2**, 021854 (2008).

[45] M. Munsch, G. Wust, A. V. Kuhlmann, F. Xue, A. Ludwig, D. Reuter, A. D. Wieck, M. Poggio, and R. J. Warburton, Manipulation of the nuclear spin ensemble in a quantum dot with chirped magnetic resonance pulses, Nat. Nanotechnol. **9**, 671 (2014).

[46] J. Dubois, U. Saalmann, and J. M. Rost, Symmetry-induced decoherence-free subspaces, Phys. Rev. Res. **5**, L012003 (2023).

[47] K. S. Cujia, J. M. Boss, K. Herb, J. Zopes, and C. L. Degen, Tracking the precession of single nuclear spins by weak measurements, Nature (London) **571**, 230 (2019).

[48] M. Pfender, P. Wang, H. Sumiya, S. Onoda, W. Yang, D. B. R. Dasari, P. Neumann, X.-Y. Pan, J. Isoya, R.-B. Liu, and J. Wrachtrup, High-resolution spectroscopy of single

nuclear spins via sequential weak measurements, Nat. Commun. **10**, 594 (2019).
[49] B. Young, B. Cabrera, A. Lee, and B. Dougherty, Detection of elementary particles using silicon crystal acoustic detectors with titanium transition edge phonon sensors, Nucl. Instrum. Methods Phys. Res., Sect. A **311**, 195 (1992).
[50] I. Alkhatib *et al.* (SuperCDMS Collaboration), Light dark matter search with a high-resolution athermal phonon detector operated above ground, Phys. Rev. Lett. **127**, 061801 (2021).
[51] W. H. Zurek, Decoherence, einselection, and the quantum origins of the classical, Rev. Mod. Phys. **75**, 715 (2003).
[52] A. S. Oja and O. V. Lounasmaa, Nuclear magnetic ordering in simple metals at positive and negative nanokelvin temperatures, Rev. Mod. Phys. **69**, 1 (1997).
[53] W. D. Knight, Nuclear magnetic resonance shift in metals, Phys. Rev. **76**, 1259 (1949).
[54] B. Urbaszek, X. Marie, T. Amand, O. Krebs, P. Voisin, P. Malentinsky, A. Högele, and A. Imamoğlu, Nuclear spin physics in quantum dots: An optical investigation, Rev. Mod. Phys. **85**, 79 (2013).
[55] G. Gillard, E. Clarke, and E. A. Chekhovich, Harnessing many-body spin environment for long coherence storage and high-fidelity single-shot qubit readout, Nat. Commun. **13**, 4048 (2022).
[56] E. A. Chekhovich, A. Ulhaq, E. Zallo, F. Ding, O. G. Schmidt, and M. S. Skolnick, Measurement of the spin temperature of optically cooled nuclei and GaAs hyperfine constants in GaAs/AlGaAs quantum dots, Nat. Mater. **16**, 982 (2017).
[57] P. Millington-Hotze, H. E. Dyte, S. Manna, S. F. C. da Silva, A. Rastelli, and E. A. Chekhovich, Approaching a fully-polarized state of nuclear spins in a semiconductor quantum dot, Nat. Commun. **15**, 985 (2024).
[58] E. A. Chekhovich, K. V. Kavokin, J. Puebla, A. B. Krysa, M. Hopkinson, A. D. Andreev, A. M. Sanchez, R. Beanland, M. S. Skolnick, and A. I. Tartakovskii, Structural analysis of strained quantum dots using nuclear magnetic resonance, Nat. Nanotechnol. **7**, 646 (2012).
[59] Q. Zhang, Y. Guo, W. Ji, M. Wang, J. Yin, F. Kong, Y. Lin, C. Yin, F. Shi, Y. Wang, and J. Du, High-fidelity single-shot readout of single electron spin in diamond with spin-to-charge conversion, Nat. Commun. **12**, 1529 (2021).
[60] T. C. Ralph, S. D. Bartlett, J. L. O'Brien, G. J. Pryde, and H. M. Wiseman, Quantum nondemolition measurements for quantum information, Phys. Rev. A **73**, 012113 (2006).
[61] W. H. Zurek, Quantum theory of the classical: Quantum jumps, Born's Rule and objective classical reality via quantum Darwinism, Phil. Trans. R. Soc. A **376**, 20180107 (2018).
[62] I. A. Merkulov, A. L. Efros, and M. Rosen, Electron spin relaxation by nuclei in semiconductor quantum dots, Phys. Rev. B **65**, 205309 (2002).
[63] M. Schlosshauer, Decoherence, the measurement problem, and interpretations of quantum mechanics, Rev. Mod. Phys. **76**, 1267 (2005).
[64] A. V. Khaetskii and Y. V. Nazarov, Spin-flip transitions between Zeeman sublevels in semiconductor quantum dots, Phys. Rev. B **64**, 125316 (2001).
[65] S. I. Erlingsson and Y. V. Nazarov, Hyperfine-mediated transitions between a Zeeman split doublet in GaAs quantum dots: The role of the internal field, Phys. Rev. B **66**, 155327 (2002).
[66] L. M. Woods, T. L. Reinecke, and Y. Lyanda-Geller, Spin relaxation in quantum dots, Phys. Rev. B **66**, 161318(R) (2002).
[67] M. Kroutvar, Y. Ducommun, D. Heiss, M. Bichler, D. Schuh, G. Abstreiter, and J. J. Finley, Optically programmable electron spin memory using semiconductor quantum dots, Nature (London) **432**, 81 (2004).
[68] C.-Y. Lu, Y. Zhao, A. N. Vamivakas, C. Matthiesen, S. Fält, A. Badolato, and M. Atatüre, Direct measurement of spin dynamics in InAs/GaAs quantum dots using time-resolved resonance fluorescence, Phys. Rev. B **81**, 035332 (2010).
[69] L. C. Camenzind, L. Yu, P. Stano, J. D. Zimmerman, A. C. Gossard, D. Loss, and D. M. Zumbühl, Hyperfine-phonon spin relaxation in a single-electron GaAs quantum dot, Nat. Commun. **9**, 3454 (2018).
[70] G. Gillard, I. M. Griffiths, G. Ragunathan, A. Ulhaq, C. McEwan, E. Clarke, and E. A. Chekhovich, Fundamental limits of electron and nuclear spin qubit lifetimes in an isolated self-assembled quantum dot, npj Quantum Inf. **7**, 43 (2021).
[71] M. Hatridge, S. Shankar, M. Mirrahimi, F. Schackert, K. Geerlings, T. Brecht, K. M. Sliwa, B. Abdo, L. Frunzio, S. M. Girvin, R. J. Schoelkopf, and M. H. Devoret, Quantum back-action of an individual variable-strength measurement, Science **339**, 178 (2013).
[72] J. H. Eberly, N. B. Narozhny, and J. J. Sanchez-Mondragon, Periodic spontaneous collapse and revival in a simple quantum model, Phys. Rev. Lett. **44**, 1323 (1980).
[73] V. Hizhnyakov, Relaxation jumps of strong vibration, Phys. Rev. B **53**, 13981 (1996).
[74] O. V. Misochko, M. Hase, K. Ishioka, and M. Kitajima, Observation of an amplitude collapse and revival of chirped coherent phonons in bismuth, Phys. Rev. Lett. **92**, 197401 (2004).
[75] A. Bassi and G. Ghirardi, Dynamical reduction models, Phys. Rep. **379**, 257 (2003).
[76] W. H. Zurek, Quantum Darwinism, Nat. Phys. **5**, 181 (2009).